

Unveiling the Potential of iMarkers: Invisible Fiducial Markers for Advanced Robotics

Ali Tourani^{1,3}, Deniz İşnsu Avşar^{2,3}, Hriday Bavle¹, Jose Luis Sanchez-Lopez¹,
 Jan P.F. Lagerwall², and Holger Voos¹ 

August 6, 2025

Abstract

Fiducial markers are widely used in various robotics tasks, facilitating enhanced navigation, object recognition, and scene understanding. While offering significant advantages for robots and Augmented Reality (AR) applications, they normally disrupt the visual aesthetics of environments because they are visible to humans, making them unsuitable for many everyday use cases. To address this gap, this paper presents “*iMarkers*”—innovative, unobtrusive fiducial markers detectable exclusively by robots and AR devices equipped with adequate sensors and detection algorithms. These markers offer high flexibility in production, allowing customization of their visibility range and encoding algorithms to suit various demands. The paper also introduces the hardware designs and open-sourced software algorithms developed for detecting *iMarkers*, highlighting their adaptability and robustness in the detection and recognition stages. Various evaluations have demonstrated the effectiveness of *iMarkers* compared to conventional (printed) and blended fiducial markers and confirmed their applicability in diverse robotics scenarios.

1 Introduction

Fiducial markers, *i.e.*, artificial landmarks with distinguishable graphical patterns, are widely used in robotics and computer vision applications to offer reliable object identification, localization, and pose estimation [1]. As markers provide better-defined reference points than naturally available ones, they are “*simple-yet-effective*” solutions where consistent feature-matching and precise pose retrieval are essential. Additionally, augmenting information via markers placed in environments and employing proper systems to extract that information can benefit a wide range of cases, including Augmented Reality (AR) and robotics tasks [2]. Markers can narrow the range of objects a robot needs to recognize and provide real-time pose information for tracking and localization. For instance, decoding data from markers detected using the robot’s camera is less costly than processing the entire visual scene that the robot can see.

Although such markers can convey various advantages in robotics, seeing multiple objects labeled with printed markers can be aesthetically undesirable and destructive. In other words, many would want to avoid seeing printed tags around them and prefer that the robots operate well without spoiling zones with these artificial landmarks. Moreover, evidence has shown that visible markers can disrupt and interrupt natural gaze behaviors [3]. Consequently, the authors worked on the idea of employing Cholesteric Spherical Reflectors (CSRs) developed by the team to produce a new generation of fiducial markers [4], dubbed *iMarker*¹. This can be done by replacing the ink pigment used in printing common fiducial markers with CSRs of spherical shell type. Due to the peculiar behavior of CSRs, *iMarkers* can be invisible (indistinguishable) to human eyes but observable by robots in case a dedicated sensor is provided [5].

¹*Authors are with the Automation and Robotics Research Group, Interdisciplinary Centre for Security, Reliability, and Trust (SnT), University of Luxembourg, Luxembourg. Holger Voos is also associated with the Faculty of Science, Technology, and Medicine, University of Luxembourg, Luxembourg. {ali.tourani, hriday.bavle, joseluis.sanchezlopez, holger.voos}@uni.lu

²*Authors are with the Department of Physics & Materials Science, University of Luxembourg, Luxembourg. {deniz.avsar, jan.lagerwall}@uni.lu

³*Authors are with the Institute for Advanced Studies, University of Luxembourg, Luxembourg.

\$*This work was partially funded by the Institute of Advanced Studies (IAS) of the University of Luxembourg (project TRANSCEND), and the Fonds National de la Recherche of Luxembourg (FNR) (project C22/IS/17387634/DEUS)

¶*For the purpose of Open Access, and in fulfilling the obligations arising from the grant agreement, the author has applied a Creative Commons Attribution 4.0 International (CC BY 4.0) license to any Author Accepted Manuscript version arising from this submission.

<https://snt-arg.github.io/iMarkers/>

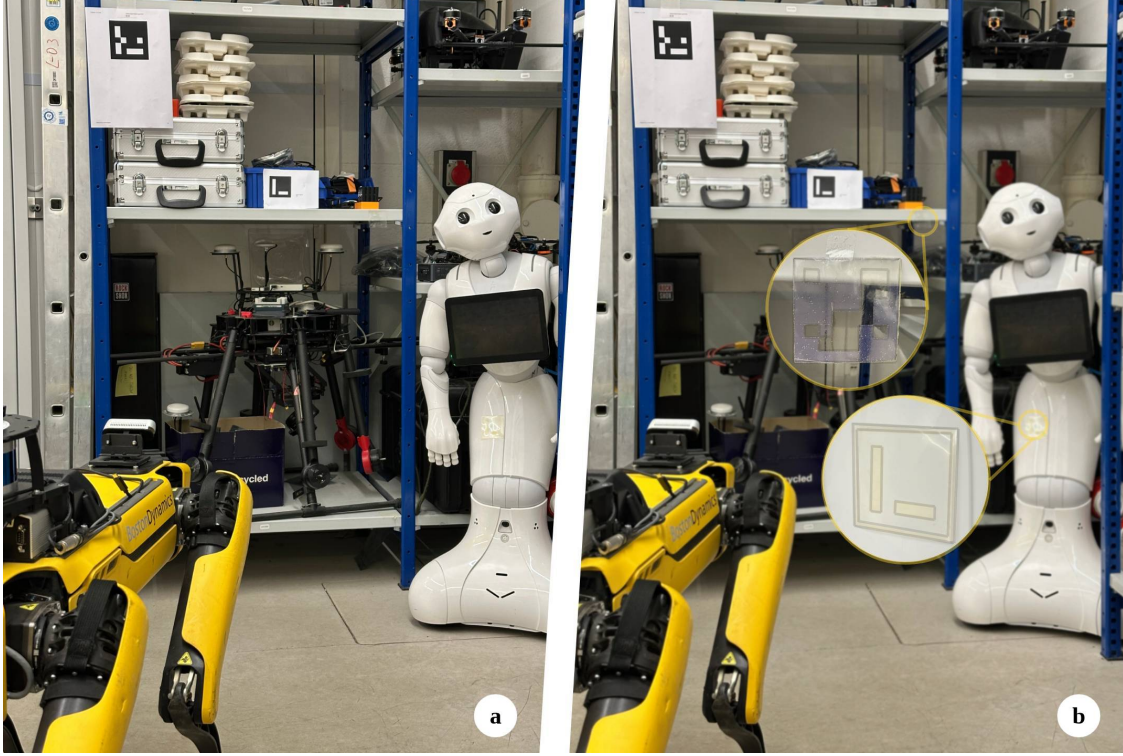


Figure 1: A legged robot observing an environment labeled with several printed fiducial markers and the proposed iMarkers: **a**) the original scene, **b**) the same scene with iMarkers highlighted and magnified.

Importantly, the sensor can be made at a very low cost. Moreover, such markers can be fabricated to be detected only within specific wavelength ranges of light, thereby avoiding visual clutter in the environment. The iMarker concept is illustrated in Fig. 1, confirming, through qualitative comparison, that they are hardly noticeable by the naked eye and in standard camera images compared to traditional printed fiducial markers.

The primary motivation of this paper is to demonstrate the potential of iMarkers in robotics by optimizing their design and detection procedure and benchmarking possible use cases in real-world robotic applications. Moreover, another objective is verifying the potential of such markers to supply simplified solutions for complex computer vision tasks in robotics, such as detecting transparent and reflective objects (*e.g.*, glass, windows, and mirrors). Hence, the leading contributions of the paper are summarized below:

- Introducing iMarkers for robotics and AR applications; invisible fiducial markers highly flexible in design and undetectable by the naked eye,
- Proposing multiple sensor solutions and software algorithms for detecting iMarkers of various designs and extracting their 6DoF pose information; and
- Assessing their potential applicability and effectiveness compared to traditional fiducial markers.

2 Literature Review

2.1 Ordinary Fiducial Markers

Fiducial marker libraries used in robotics and AR applications are expected to enable rapid detection, reliable recognition, and efficient information decoding. Ordinary fiducial markers, mainly printed on paper, can be classified into non-square (designed as circles, point sets, or arbitrary visual patterns), square (or matrix-based), and hybrid variations. In non-square markers, identification and data decoding generally occur w.r.t. the center of their geometric

shape. InterSense [6] and WhyCode [7] are circular-shaped libraries in which the correspondence point detection is the tricky part. Dot-shaped libraries, such as RUNE-Tag [8], supply fast detection but suffer primarily in noisy conditions. Other arbitrary and shape-free markers are mainly used in 6-Degrees-of-Freedom (6DoF) feature tracking and pose estimation. Despite robust detection, the mentioned method faces challenges like inter-marker encoded dot confusion and steep viewing angle recognition.

Square fiducial markers, on the other hand, employ binary codes encoded in matrices and deliver four principal corner points for more precise pose estimation. They require less computation cost for detection and recognition, leading to potentially faster detection algorithms. ARToolkit [9] is an open-source matrix-based marker library that uses template-matching for square marker pattern determination. However, it may face high re-projection errors with rotation and camera angle changes. AprilTag [10] is another marker library that incorporates gradient-based edge detection and reliable line identification to ensure accurate marker recognition, even under challenging viewing angles. Its enhanced digital coding system has made it more robust to rotation, occlusion, and warping compared to traditional systems, such as ARToolkit. Similarly, Garrido-Jurad *et al.* introduced ArUco Marker [11] that generates configurable marker dictionaries with maximized inter-marker distances. Their system contains automatic marker detection with error correction based on dictionary search and a novel occlusion handling method using color-based occlusion masks for robust pose estimation.

Despite their widespread use and robust performance, these markers, whether non-square or square, remain visually intrusive and can disrupt environments' natural aesthetics. This limitation has motivated the development of markers that blend more seamlessly into their surroundings.

2.2 Blended and Unobtrusive Fiducial Markers

In contrast with ordinary paper-based markers, some solutions propose fiducial markers for particular scenarios that require special sensors to be detected. In this regard, ArTuga [12] is a multimodal marker that targets detection in challenging environments by photometric and radiometric sensor fusion, mainly designed to enhance the precise landing of drones in harsh environments. Seedmarkers [13] consider the aesthetic properties of fiducial markers by embedding them in physical objects, ranging from laser-cut plates to 3D-printed tangibles. ACMarker [14] is another solution to create fiducial markers detectable using customized sensors for underwater robotics applications.

Several approaches focus on integrating less obtrusive markers into environments to minimize their visual impact while maintaining robust detectability. Transparent Random Dot Marker [15] is an approach that aims to keep markers on transparent sheets with small randomly placed printed dots, making them barely visible in ordinary scenarios. Nevertheless, geometric point matching and marker detection can be tricky while integrating pairwise relationships among the detected dots. InfraredTags [16] are discreet and durable markers designed to be printed and embedded within various objects, offering invisibility and rapid scanning. However, their production is limited to the Infrared (IR) range, restricting flexibility in fabrication. Additionally, their thin and embedded nature makes them difficult for users to locate, complicating the process of directing IR torches or cameras for detection. Similarly, BrightMarkers [17] are 3D-printed fluorescent filaments embedded into objects, which require Near Infrared (NIR) cameras for detection. Aircode [18] introduced the concept of embedding markers directly into the fabrication of objects, enabling seamless integration for use cases such as robotic grasping. Nevertheless, Aircode's significant drawback is its slow decoding process, which can take tens of seconds, depending on the camera's viewing angle.

2.3 Gap Identification

Although the surveyed blended and unobtrusive methodologies have indicated effectiveness in robotics and AR tasks by keeping markers discreet, their applicability in real-world scenarios is often restricted by the trade-off between “*invisibility*” and “*detection speed*.” In other words, solutions like AirCode achieve high levels of invisibility but suffer from significantly slow detection speeds. Other crucial factors include simplicity, cost-effectiveness, detection versatility, and robust performance, as well as fabrication flexibility across various light spectra. These dimensions significantly influence the adoption of such fiducial marker solutions compared to the straightforward and easily printable traditional markers.

Table 1: A comparison of the primary features and capabilities of various unobtrusive fiducial marker solutions.

	AirCode [18]	InfraStructs [19]	InfraredTags [16]	iMarker (ours)
<i>Unobtrusiveness to human</i>	✓	✓	✓	✓
<i>Core material</i>	air pockets	polystyrene	IR filament	CSRs
<i>Versatile pattern coding</i>	✗	✗	✓	✓
<i>Fabrication cost</i>	high	normal	low	low
<i>Fabrication simplicity</i>	✗	✗	✓	✓
<i>Production versatility *</i>	Vis, UV	IR	IR	IR, UV, Vis
<i>Sensor cost</i>	very high	high	low	low
<i>Detection time range</i>	second	second	millisecond	millisecond

*IR, UV, and Vis refer to Infrared, Ultraviolet, and visible ranges, respectively.

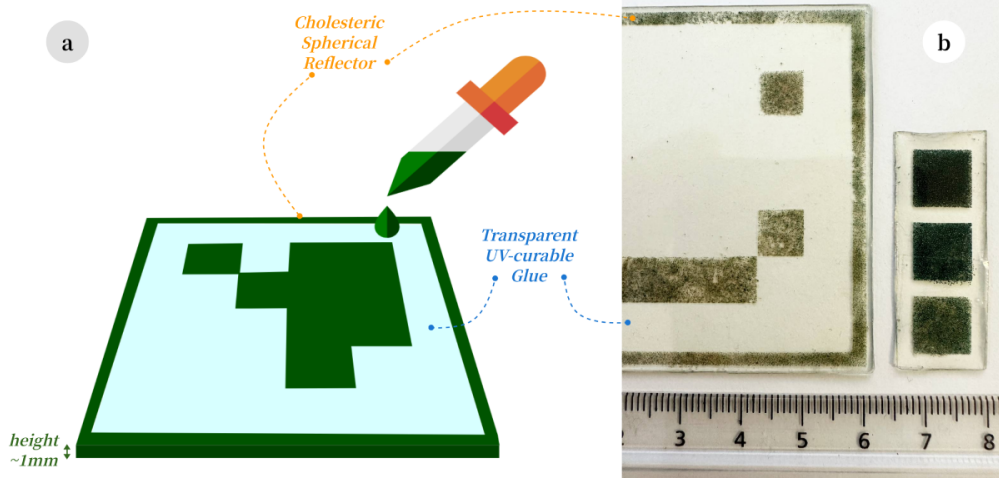


Figure 2: The role of CSRs in the design of iMarkers: **(a)** an iMarker featuring ArUco patterns filled with CSRs, **(b)** an iMarker displayed next to visible CSR particles, illustrating various shades of green for fabrication.

3 iMarkers: Concept and Comparison

iMarkers [5] present an innovative and versatile solution to address the mentioned gaps by ensuring transparency, flexibility, and unobtrusiveness. Given the proper sensor and detection algorithm, they can be fabricated to achieve high contrast for detection while remaining undetectable to the naked eye. Thus, they improve fiducial markers' functionality and visual harmony in various settings. Table 1 highlights the characteristics of iMarkers compared to other methodologies aimed at seamlessly blending markers into their surroundings. According to the table, although all solutions aim to remain hidden from human perception, iMarkers cover distinct aspects that set them apart, as outlined below:

Core Material: The primary material used to make iMarkers is CSRs, microscopic droplets of Cholesteric Liquid Crystals (CLCs) that self-organize into a helical structure, making them highly effective at reflecting specific wavelengths of light, including IR, Ultraviolet (UV), or visible [5]. Their spherical shape turns them into omnidirectional selective retroreflectors, ensuring they can be easily detected regardless of viewing angle. Thus, they can produce vivid, circularly polarized iridescent colors resulting from the selective reflection of light. As shown in Fig. 2, iMarkers combine CSRs for the marker patterns with transparent UV-curable glue to maintain the structure of the fiducial marker. An alternative fabrication method involves directly spraying CSR shells onto surfaces, a promising approach currently under investigation.

Pattern Coding and Recognition: iMarkers support various coding patterns for recognition and information retrieval. This paper focuses on ArUco-based [11] markers with variant dictionaries, but other standard fiducial marker libraries can also be adapted to the iMarker design.

Fabrication Efficiency: The cost and simplicity of fabrication significantly impact the widespread adoption of



Figure 3: Versatility in iMarker production: **(a)** a $6 \times 6 \text{ cm}^2$ UV-range iMarker, **(b)** an IR-range iMarker with the same size, **(c)** the UV-range iMarker placed on a transparent surface, **(d)** a $7 \times 7 \text{ cm}^2$ dark green visible-range iMarker camouflaged with its background.

fiducial markers. While AirCode requires partitioning and InfraStructs depend on complex, layered assembly, iMarkers, as shown in Fig. 2, can be fabricated using cost-effective methods like dispensing or spray coating.

Production Versatility: In contrast with other solutions, iMarkers offer production flexibility, enabling design and detection across the entire light spectrum. UV-range iMarkers remain entirely transparent and invisible to the naked eye, even when positioned on a transparent surface like glass. IR-range iMarkers are similarly discreet, though slight scattering or subtle color effects may reveal their presence (to some extent) under extreme lighting conditions. Even in the visible range, iMarkers can be designed to blend with patterned backgrounds or camouflage against similarly colored surfaces, ensuring minimal visual intrusion. Fig. 3 depicts actual examples of iMarkers made from different CSR shells.

Sensor Affordability: Detection requirements differ among unobtrusive marker solutions: AirCode relies on a large projector and camera setup, InfraStructs require costly Terahertz scanners, and InfraredTags depend on specialized imaging modules with microprocessors. In contrast, iMarkers can be detected using affordable sensors with standard optical components. The camera for detecting iMarkers must be compatible with the polarization and wavelength characteristics of the CSRs employed in its fabrication.

Detection Algorithm Performance: Since the sensors are designed to generate binary images, fiducial marker patterns are detected within milliseconds, ensuring real-time performance for various robotics and AR use cases.

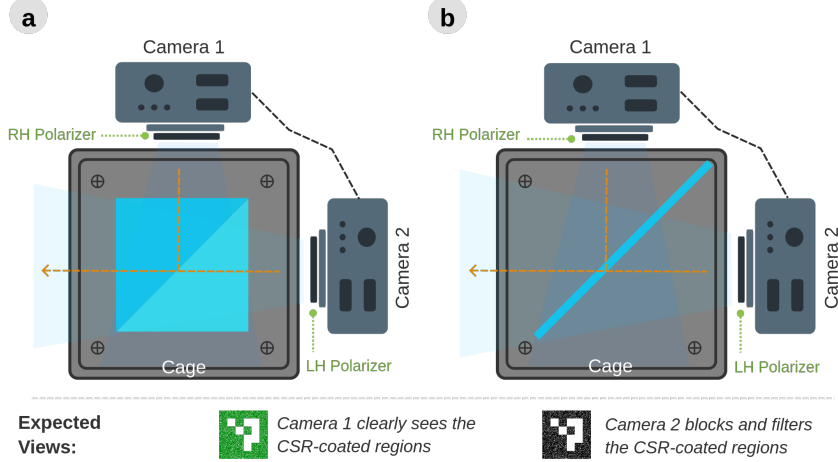


Figure 4: Dual-vision setup variants designed for iMarker detection, each containing two synchronized cameras with attached circular polarizers to their lenses facing a cube (a) or plate (b) beamsplitter.

4 Sensor Design and Detection Strategies

Considering the versatility of iMarkers, a range of perception sensors and detection algorithms can be employed to ensure reliable recognition across diverse applications. Hence, three primary solutions are proposed for iMarker detection, including “*dual-vision*,” “*dynamic single-vision*,” and “*static single-vision*,” which are further described in the following:

4.1 Dual-vision Solution

Sensor Design. The first sensor is a homogeneous perception system containing two perpendicularly positioned synchronized cameras, each facing a different surface of an optical beamsplitter. As shown in Fig. 4, the sensor can be assembled in two variants: one using a cube and the other employing a plate beamsplitter. The beamsplitter divides the incoming light equally (*i.e.*, 50:50) into two parts, including the transmitted (that passes through) and the reflected light. Thus, by mounting the cameras and beamsplitter within a cage setup, one camera captures the scene using the transmitted light, while the other captures it using the reflected light, resulting in two perspectives with minimal variation. Attaching identical circular polarizers to each camera’s lens effectively blocks light with the opposite circular polarization, ensuring only the desired handedness is detected.

Due to the inversion of circular polarization upon reflection in the beamsplitter, the camera capturing the reflected light detects the “opposite” circular polarization compared to the camera capturing the transmitted light. Accordingly, the sensor simultaneously captures the same scene with two cameras, ensuring that the CSR regions of iMarkers in the sensor’s Field of View (FoV) appear blocked in one camera while remaining visible in the other (due to the opposing circular polarization of the CSR reflections).

The cameras in this setup must be synchronized to capture the same scene simultaneously. Simplistically, frame $f_t^{C_1}$ captured by camera C_1 at time t should depict the same scene as frame $f_t^{C_2}$ of camera C_2 . Additionally, as the cameras’ frame rate and shutter speed are vital factors for high-speed robotic applications (*e.g.*, drone navigation), integrating global shutter cameras in this sensor is highly recommended. The calibration procedure for the setup involves capturing a standard calibration pattern (*e.g.*, a chessboard) by each camera individually and with the entire sensor system. The camera’s intrinsic (*e.g.*, focal length and distortion coefficients) and extrinsic parameters are required for iMarker pose estimation.

Detection Algorithm. Since the non-CSR regions of the scene lack circular polarization and appear identical in both cameras, it enables the use of simple computer vision techniques (*e.g.*, image subtraction) to detect iMarkers with high contrast, as detailed in [5] and shown below. As shown in Algorithm 1, the iMarker detection procedure requires “*spatial subtraction*” of the synchronized frames captured by each camera. Having \mathbf{F}_{C_1} and \mathbf{F}_{C_2} as the synchronized frame sets captured by calibrated cameras C_1 and C_2 , each frame $f_1 \in \mathbf{F}_{C_1}$ finds its corresponding synchronized frame $f_2 \in \mathbf{F}_{C_2}$. The next stage is aligning f_2 based on f_1 using the alignment parameters h (captured during calibration),

Algorithm 1 Dual-vision iMarker detection.

Require: frame-sets F_1 and F_2 from cameras C_1 and C_2
Ensure: list of detected fiducial markers M

```

 $M \leftarrow []$ 
 $p_1 \leftarrow \text{calibrate } C_1$ 
 $p_2 \leftarrow \text{calibrate } C_2$ 
 $h \leftarrow \text{align } (F_1, F_2) \text{ considering } p_1 \text{ and } p_2$ 
while  $f_1$  in  $F_1$  do
     $f_2 \leftarrow \text{corresponding sync frame in } F_2$ 
     $f_2 \leftarrow \text{align } f_2 \text{ based on } f_1 \text{ using } h$ 
     $f_p \leftarrow f_2 - f_1 \text{ \{final subtracted image\}}$ 
     $f_p \leftarrow \text{threshold } f_p$ 
     $f_p \leftarrow \text{post-process } f_p \text{ \{erosion + Gaussian blur\}}$ 
    if marker  $m$  found in  $f_p$  then
        add  $m$  to  $M$ 
    end if
end while
return  $M$ 

```

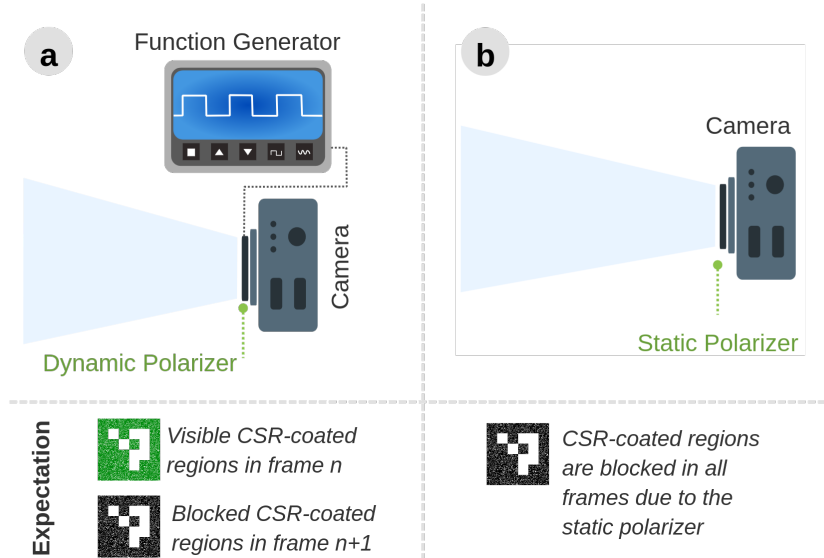


Figure 5: Single-vision setup variants designed for iMarker detection, each containing a camera with attached dynamic (a) or static (b) polarizers.

where h is the homography matrix generated through matching Oriented FAST and Rotated BRIEF (ORB) features. Subtracting the “aligned” f_2 from the “original” f_1 frame results in the final binary image f_p containing the input images’ dissimilar parts. Since the CSR region of iMarkers is visible in one frame and blocked in the other, only the patterns created by CSRs are expected to remain in f_p . Then, a thresholding process with a value of θ , followed by post-processing, is applied to f_p to generate a binary frame that enhances the iMarker patterns’ visibility. The final processed frame contains potential iMarkers $m \in \mathbf{M}$, where \mathbf{M} is the set of iMarkers found in f_1 and f_2 at time t .

4.2 Dynamic Single-vision Setup

Sensor Design. The second approach offers a solution for iMarker detection using a single camera equipped with a switchable (dynamic) circular polarizer alternating between left- and right-handed polarization (Fig. 5-a), which will be described in detail in a forthcoming paper. In brief, it comprises a fixed circular polarizer paired with a nematic liquid crystal film that functions as a $\lambda/2$ -plate in its relaxed (OFF) state and loses its optical functionality when an electric field is applied (ON). A $\lambda/2$ -plate converts one circular polarization to its opposite; therefore, by switching the liquid crystal film between its ON and OFF states (controlled by a function generator synchronized with the camera’s frame rate), the camera sequentially captures frames with right- and left-handed polarization, separated in time. In an ideal setup, camera frame f_t captures the scene with a particular polarization (left- or right-handed), and frame f_{t+1} captures it with the opposite polarization. Thus, the function generator should send signal S_g to trigger the liquid

Algorithm 2 Dynamic single-vision iMarker detection.

Require: frame-set F from the camera
Ensure: list of detected fiducial markers M

```

 $M \leftarrow []$ 
 $f_{prev} \leftarrow null$ 
while  $f_t$  in  $F$  do
   $f_p \leftarrow f_t - f_{prev}$  {final subtracted image}
   $f_p \leftarrow$  post-process  $f_p$  {erosion + Gaussian blur}
   $f_{prev} \leftarrow f_t$ 
  if marker  $m$  found in  $f_p$  then
    add  $m$  to  $M$ 
  end if
end while
return  $M$ 

```

crystal film at time t based on Equation 1:

$$S_g = \begin{cases} \text{on}, & \text{for } t = 1, 3, \dots, 2n - 1, \\ \text{off}, & \text{for } t = 2, 4, \dots, 2n. \end{cases} \quad (1)$$

The liquid crystal cell's OFF-to-ON switching time is negligible and can be ignored; however, the ON-to-OFF relaxation is slower. Thus, the intermediate frames with undefined polarization for high frame rates may need to be discarded for the iMarker detection procedure. Once optimized for the liquid crystal cell, it ensures that CSR-coated regions in the iMarkers are blocked in one processed frame and visible in the next.

Detection Algorithm. Inspired by the “spatial” frame processing in the dual-vision setup, this approach employs a frame-level algorithm that uses “temporal” subtraction to detect the iMarker patterns. Assuming the liquid crystal film operates sufficiently fast relative to the video frame rate to produce sequential frames with alternating polarization states (as illustrated in Equation 1), the consecutive (temporal) frame subtraction algorithm to detect iMarkers using a switchable polarizer is shown in Algorithm 2. In this process, each frame f_{t-1}^{off} and its subsequent frame f_t^{on} , captured with alternating polarization states, are subtracted to produce a grayscale image f_p , which can then be enhanced through post-processing to facilitate iMarker detection. Additionally, the current frame is stored for subtraction from its succeeding frame in the next iteration. As with the previous approaches, the final stage involves detecting fiducial markers M within the processed frame f_p .

4.3 Static Single-vision Setup

Sensor Design. Another configuration offers a solution for iMarker detection using a single camera equipped with a static circular polarizer attached to its lens (Fig. 5-b). The polarizer is selected to block the circular polarization reflected by the CSRs forming the iMarker pattern. For instance, a left-handed circular polarizer will block iMarker regions with CSRs reflecting right-handed polarization, and vice versa. Thus, a visible-range iMarker with CSRs reflecting right-hand polarized light on a same-color background (*e.g.*, green, blue, *etc.*), indistinguishable to the human eye or standard cameras, becomes detectable as the sensor's left-handed polarizer blocks the CSR regions, revealing the camouflaged iMarker patterns. This design is well-suited for detecting visible-range iMarkers camouflaged within their environment, while it can also be used for IR/UV-range iMarkers using proper cameras.

Detection Algorithm. Unlike the dual-vision solution, the algorithm for the static single-vision setup does not eliminate the background. However, it simplifies constructing and integrating an iMarker detection sensor by shifting more computation to the detector methodology, achieving a practical balance between complexity and performance. For the visible-range camouflaged iMarkers, the procedure is shown in Algorithm 3. Accordingly, detecting iMarkers M in a frame $f \in \mathbf{F}$ involves converting f from *RGB* to *HSV* color space to isolate the color range corresponding to the marker. The resulting mask frame f_p highlights the target color range c_r as black pixels, with all other areas appearing as white. With the assistance of the polarizer, the mask frame f_p highlights the blocked CSR regions of an iMarker with color c (*e.g.*, green) positioned against a background of the same color. Subsequent stages of the algorithm apply post-processing to eliminate noise, followed by detecting marker patterns M within f_p .

Detecting UV/IR-range iMarkers follows the same stages as the visible-range detection, provided that a UV/IR-range camera is used. However, “color masking” is unnecessary since the input is grayscale, and “range thresholding” is applied to identify the intensity variations in CSR regions, highlighting the iMarker patterns. Thus, Algorithm 4 can be employed for UV/IR-range iMarker detection scenarios.

Algorithm 3 Static single-vision iMarker detection (masking).

Require: frame-set F from the camera (*RGB*)
Ensure: list of detected fiducial markers M

```
 $M \leftarrow []$ 
 $r \leftarrow (low, high)$  {demanded color range in HSV}
while  $f$  in  $F$  do
   $f_p \leftarrow$  convert  $f$  to color space HSV
   $f_p \leftarrow$  filter  $f_p$  with the range  $r$ 
   $f_p \leftarrow$  post-process  $f_p$  {erosion + Gaussian blur}
  if marker  $m$  found in  $f_p$  then
    add  $m$  to  $M$ 
  end if
end while
return  $M$ 
```

Algorithm 4 Static single-vision iMarker detection (thresholding).

Require: frame-set F from the camera (*grayscale*)
Ensure: list of detected fiducial markers M

```
 $M \leftarrow []$ 
 $r \leftarrow (low, high)$  {demanded gray-level range in grayscale}
while  $f$  in  $F$  do
   $f_p \leftarrow$  filter  $f_p$  with the range  $r$ 
   $f_p \leftarrow$  post-process  $f_p$  {erosion + Gaussian blur}
  if marker  $m$  found in  $f_p$  then
    add  $m$  to  $M$ 
  end if
end while
return  $M$ 
```

5 Benchmarking and Evaluation

This section explores the potential and applicability of iMarkers from various aspects of real-world scenarios.

5.1 Operational Implementation

Considering the iMarker detection strategies outlined in Section 4, real-world sensor employment and algorithm implementation are the focus of this subsection to form the basis for subsequent evaluations.

Sensor. Fig. 6 depicts the different sensor configurations developed for iMarker detection. The dual-vision setup shown in Fig. 6-a comprises two ELP 8MP HD camera modules with 75° FoV facing a Thorlabs polarizing cube beamsplitter with a 50:50 split ratio, all mounted in a compact cage assembly. The other dual-vision setup in Fig. 6-b contains two synchronized U3-3271LE iDS cameras aligned with a Thorlabs polarizing plate beamsplitter housed within a custom-designed 3D-printed cage. The static single-vision setup shown in Fig. 6-c is an Intel® RealSense™ D435 camera equipped with a left-handed circular polarizer affixed to its RGB lens, effectively blocking the right-handed CSR-coated areas of camouflaged iMarkers. Finally, the dynamic single-vision sensor setup in Fig. 6-d incorporates a switchable polarizer controlled by a function generator mounted on an iPhone 13 case and aligned with its camera. While this prototype relies on manual polarizer switching, we are investigating a real-time version where the detection software dynamically synchronizes the camera and function generator to adjust polarization (left- or right-handed).

Software. To support the detection algorithms outlined in Section 4, an open-sourced ² iMarker detection software framework has been developed. The framework is implemented in Python and features a ROS2 interface, enabling straightforward integration into robotic applications.

5.2 Qualitative Evaluation

Given the complexity of measuring aesthetic perception, this section aims to visually assess iMarkers and showcase their detection performance. To achieve this, various iMarkers were strategically placed in rigid real-world locations and captured using different hardware sensors, highlighting their seamless integration into diverse settings. It should be noted that while aesthetic perception is inherently subjective, the visual comparisons provided in Fig. 1 and Fig. 3 offer practical, real-world evidence supporting the unobtrusiveness of iMarkers in diverse environments.

²<https://snt-arg.github.io/iMarkers/>

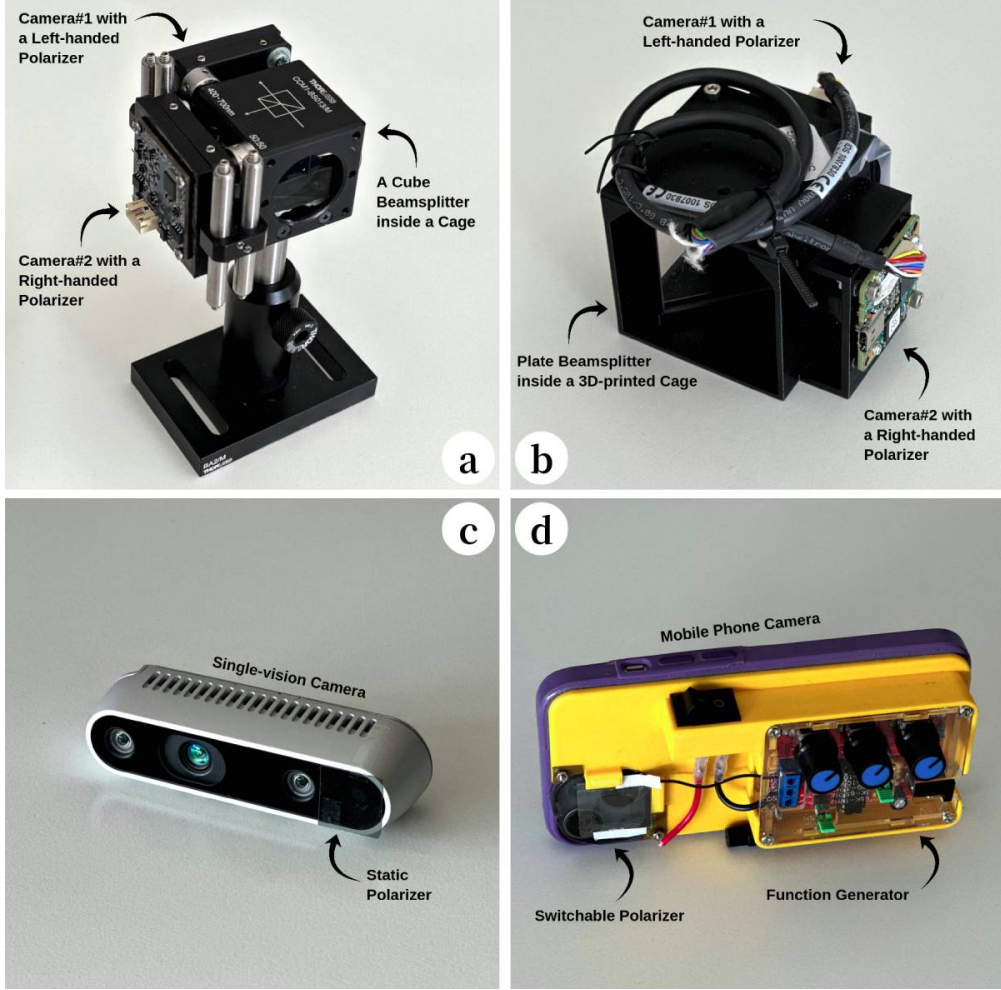
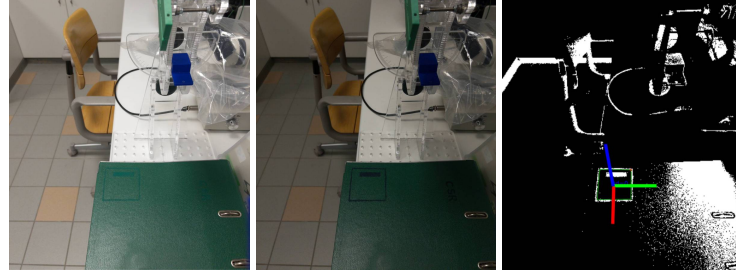


Figure 6: Variant iMarker detection sensors, including the dual-vision setup with cube (a) and plate (b) beamsplitters, and single-vision setups with static (c) and dynamic (d) polarizers.

Fig. 7 depicts several qualitative results, showing the versatility of iMarkers across different spectral ranges and detection setups. Accordingly, Fig. 7a presents a visible-range green iMarker discreetly embedded on a similar color background, demonstrating its visual camouflage and unobtrusiveness. In this scenario, the static single-vision setup was employed to capture the scene, where the setup’s polarizer effectively blocks the CSR regions forming the inner iMarker pattern, enhancing the contrast and enabling enhanced separation for detection. The detection and pose estimation outcome was obtained using Algorithm 3. Fig. 7b and Fig. 7c depict the output of the dynamic single-vision setups applied to the same visible-range iMarker in indoor and outdoor conditions. Detection is achieved through temporal subtraction between frames f_{t-1}^{off} and f_t^{on} following the procedure described in Algorithm 2. In Fig. 7d, the output of the dual-vision setup targeting a visible-range iMarker placed on a patterned surface under low-light conditions is shown. In this configuration, both cameras simultaneously capture the same scene, with the left camera acquiring frame f_l through a left-handed polarizer and the right camera capturing frame f_r through a right-handed polarizer. Marker detection was performed using Algorithm 1, which applies spatial subtraction between the polarized image pairs. Finally, the UV-range iMarker placed on a transparent surface depicts exceptional invisibility to the naked eye, as illustrated in Fig. 7e. To reveal the inner patterns of the iMarker, a near-UV illumination was applied, and the same scene was captured using the UV-range camera, as shown in the middle sub-figure. The methodology introduced in Algorithm 4 facilitates the marker detection process by applying a tailored thresholding strategy to the UV image, enabling reliable iMarker’s invisible patterns extraction.



(a) Static single-vision setup detecting a visible-range iMarker: raw frame (left), polarizer applied (middle), and detection result using color masking (right).



(b) Dynamic single-vision setup detecting a visible-range iMarker: frames f_{t-1}^{off} (left) and f_t^{on} (middle) captured at different times with alternating polarizer states, and the detection result obtained via temporal subtraction (right).



(c) Dynamic single-vision setup detecting a visible-range iMarker in an outdoor environment. The order of the frames (off-polarized, on-polarized, and subtraction) follows the same structure as (b).



(d) Dual-vision setup capturing a visible-range iMarker under low-light conditions: frames f_l (left) and f_r (middle) acquired using orthogonal polarizers, and the detection result obtained via spatial frame subtraction $f_l - f_r$ (right).



(e) Single-vision UV iMarker detection: scene as captured by a standard mobile phone camera (left), corresponding view captured with a UV-sensitive camera under near-UV illumination (middle), and the resulting marker pattern revealing output via thresholding (right).

Figure 7: iMarker variants detected using different sensor setups and corresponding algorithms, including the visible- and UV-range iMarkers.

5.3 Detection Range and Pose Accuracy Evaluation

To evaluate the effectiveness of iMarkers against their classic paper-printed counterparts, a series of comparative experiments were conducted using both marker variants in the ArUco format. The experiments focused on two primary objectives: (1) determining the maximum detection range across varying viewing angles, and (2) assessing the accuracy of the estimated 6DoF pose for each marker type; both were done using the ArUco detection algorithm. The employed sensor across all scenarios was the single-vision setup with Intel® RealSense™ D435, unmodified for printed markers and equipped with static/dynamic polarizers for iMarker detection. We intentionally limited the analysis to this setup to ensure fair comparison for detecting printed markers and iMarkers, while other sensors in Fig. 6 differ significantly in resolution, shutter type, and optical characteristics. All experiments were conducted using the camera’s RGB sensor at a resolution of 1024×768 to maintain uniform input quality across evaluations. Regarding marker dimensions, $7 \times 7 \text{ cm}^2$ visible-range iMarker variants were used to be compared against $6 \times 6 \text{ cm}^2$ and $7 \times 7 \text{ cm}^2$ printed ArUco marker references. Evaluations were performed under normal lighting conditions and in a controlled robotics laboratory equipped with an OptiTrack motion capture system, providing sub-millimeter ground truth accuracy for 6DoF pose tracking. Both the printed fiducial markers and the fabricated iMarkers were affixed to a tripod with an adjustable mounting plate, allowing precise control over their orientation relative to the camera. To ensure accurate ground truth acquisition during the evaluations, omnireflective motion capture landmarks were placed on both the fiducial markers, with their poses continuously tracked using the OptiTrack system. The examined viewing angle ranged from 0° to 75° , within which the estimated poses of the markers remained reliable w.r.t. the ground truth.

Maximum detection range. According to the evaluation results in Fig. 8, increasing the viewing angle reduces the maximum marker detection range in all scenarios, mainly due to perspective distortion. Additionally, iMarker detection using static and dynamic single-vision setups shows negligible differences in maximum detection ranges, differing between 3 cm to 7 cm, with an average of 4.82 cm. However, regardless of the detection setup, printed markers achieved consistently higher detection ranges than iMarkers of identical dimensions ($7 \times 7 \text{ cm}^2$). The detection range of $7 \times 7 \text{ cm}^2$ iMarkers closely matches that of $6 \times 6 \text{ cm}^2$ printed ArUco markers, with differences ranging from 4.12 cm to 6.39 cm and averaging 4.24 cm across various angles of view. It should be noted that printed ArUco markers, thanks to their high-contrast black-and-white patterns, offer substantial visual features that facilitate detection. However, iMarkers demonstrate comparable detection performance in real-world experiments, apart from their distinct advantage over classic markers: their ability to seamlessly blend into the environment without disrupting visual aesthetics. This makes iMarkers highly suitable for shorter-range applications where visual discretion is essential, such as indoor navigation.

Pose accuracy. The pose estimation accuracy was assessed by measuring the deviation of the detected marker poses from ground truth data under the mentioned viewing angles. As shown in Table ??, *the mean pose estimation error norm across various viewing angles remains consistent among the printed ArUco markers and their iMarker counterparts. In general, the detection error increases as the viewing angle grows from 0° to 75°* due to increasing perspective distortion of the marker appearance. The relative difference in pose estimation error between printed markers and iMarkers remains within a narrow range of 1.3% to 3.9%. This consistency and negligible error differences were expected outcomes of our system design, as the proposed hardware-software configurations are explicitly designed to produce pre-processed binary images revealing the marker patterns prior to the *detection and pose estimation* stage in the standard ArUco detector library. Thus, the marker detector library can recognize both types of markers by applying built-in preprocessing to either standard RGB inputs of printed markers, or the binary outputs generated by the iMarker detection system.

5.4 Recognition Speed

Considering the necessity of fast recognition speeds in demonstrating the practicality of fiducial markers for real-time applications, this subsection provides a detailed profiling analysis of iMarker detection and recognition. Table 2 summarizes cumulative processing times for iMarker data decoding. Evaluations were conducted using various sensor configurations and implemented software introduced in subsection 5.1. The algorithms developed for all sensor variants share five core modules: “*acquisition*,” which captures video frames; “*preprocessing*,” which applies image enhancement techniques; “*processing*,” which refines frames to emphasize marker patterns; “*post-processing*,” which enhances the final binary images; and “*recognition*” to detect and interpret marker patterns. To obtain the measurements, $7 \times 7 \text{ cm}^2$ iMarkers were placed approximately 50 cm from the lens, directly facing the sensor under standard lighting conditions with evenly diffused artificial illumination. For the UV-range iMarker, a DARKBEAM A300 365 nm flashlight was additionally used to enhance the iMarker visibility.

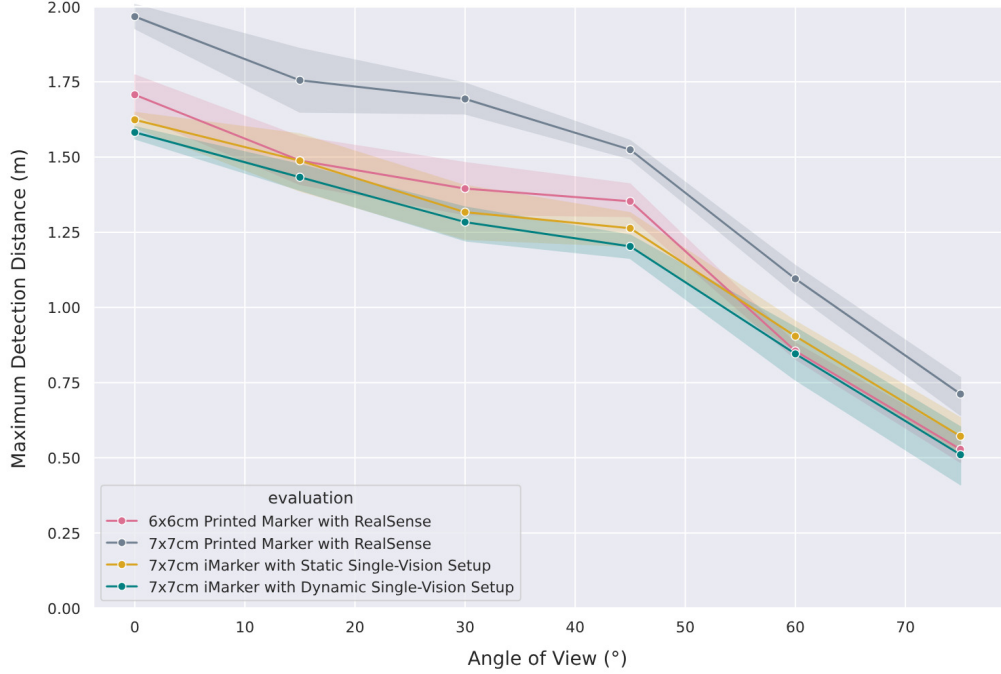


Figure 8: Maximum detection distances for “printed” and “iMarkers” ArUco formats at various viewing angles. The shaded regions (error bands) indicate measurement uncertainty in maximum recognition distance.

According to Table 2, the overall iMarker recognition process, from video frame “*acquisition*” to inner pattern “*recognition*” steps, is completed within milliseconds. To compare, some methods discussed in Table 1 require several seconds for detection, highlighting the efficiency of the iMarker system. Among the various configurations, UV-range iMarker recognition (Algorithm 4) is the fastest, as the input image is already in grayscale, requiring only a simple “*thresholding*” operation to reveal the marker pattern for recognition. In dual-vision setups (Algorithm 1), “*acquisition*” and “*processing*” account for the subsequent significant portions of the processing time due to the need to receive synchronized frames from two cameras and perform image alignment for further processing, respectively. The “*post-processing*” stage is executed more efficiently, as the substantial filtering process retains only the differing image regions, *i.e.*, the CSR areas. On the other hand, single-vision setups operate faster in “*acquisition*” due to capturing frames from a single camera. However, they allocate more time to “*post-processing*”, as the captured images contain higher noise levels and the need to refine iMarker regions effectively.

6 Discussion

6.1 Comparative Insights

Fig. 9 depicts relative performance scores of different iMarker fabrication variants and the designed sensor configurations for their detection, where larger areas indicate higher values. The relative performance scores were assigned based on theoretical analysis and experimental observations, which will be described in detail.

In Fig. 9-a, three primary performance aspects of the iMarker variants have been analyzed. Regarding “invisibility,” UV-range iMarkers remain entirely imperceptible to the eye, while IR-range iMarkers may exhibit slight visibility due to scattering under extreme lighting conditions. Visible-range iMarkers, on the other hand, are designed to blend into patterned backgrounds; however, upon close inspection, they remain minimally visible to the human eye. When “readability” is studied, visible-range iMarkers have better compatibility with standard cameras and do not require additional illumination. However, IR- and UV-range iMarkers require dedicated illumination sources and particular sensors, with varied detection performance based on environmental conditions. Finally, and in terms of “detection equipment cost” (camera, flashlight, *etc.*), visible-range iMarkers are the most economical, as they can be detected using standard cameras. UV equipment (camera and illumination sources) is generally the most expensive among the

Table 2: Performance analysis of iMarkers detection and recognition, based on cumulative time profiling of required modules (averaged over 40 frames) in milliseconds (ms). Abbreviations are detailed below the table.

Software Module	iMarker Variant				
	UV	Visible-range			
SV Static	SV Static	SV Dynamic	DV (cube BS)	DV (plate BS)	
Acquisition	11 ms	15 ms	13 ms	32 ms	36 ms
Preprocessing	2 ms	7 ms	9 ms	14 ms	19 ms
Processing	3 ms	23 ms	29 ms	39 ms	42 ms
Post-processing	3 ms	9 ms	8 ms	4 ms	5 ms
Recognition	2 ms	2 ms	3 ms	2 ms	3 ms
Sum	21 ms	56 ms	62 ms	91 ms	105 ms

*PS. *SV*: Single-Vision, *DV*: Dual-Vision, *UV*: Ultraviolet, *BS*: Beamsplitter

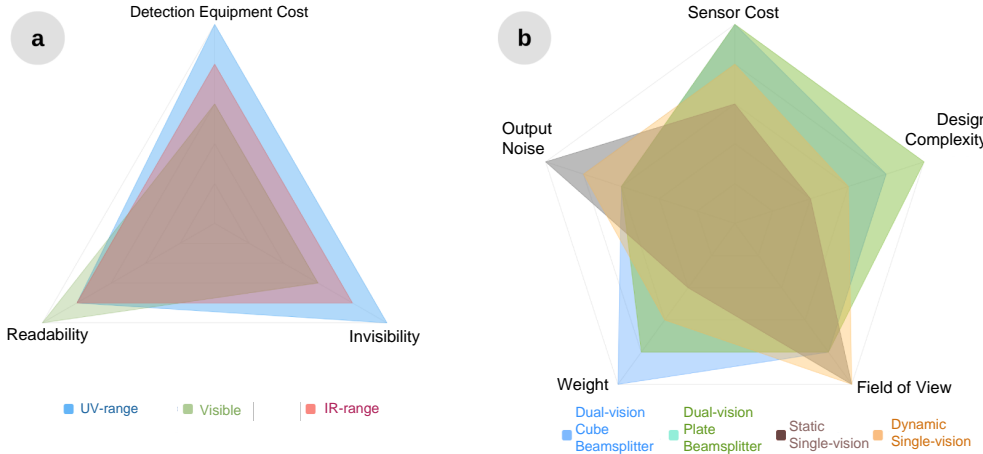


Figure 9: Relative performance scores of iMarker variants (a) and sensors (b) across multiple aspects, with larger areas indicating higher values. The term “BS” stands for beamsplitter.

three, and IR-range iMarker detection equipment cost lies in between.

Considering the sensor-related factors shown in Fig. 9-b, the performance scores can be studied in five aspects. In “design complexity,” the static single-vision setup is the most straightforward, requiring only a static polarizer attached to the lens. The dynamic single-vision setup has moderate complexity by incorporating a function generator to control polarization. Dual-vision configurations represent the most complex designs, with the cube beamsplitter offering more reliable light division than the plate one, which requires precise alignment for optimal beam splitting. The design complexity directly influences the “sensor cost.” The static single-vision setup offers the most economical solution, requiring only a polarizer, while the dynamic single-vision configuration incurs additional costs due to its polarization control components. Dual-vision setups are generally more expensive. They require two cameras, a beamsplitter (either cube or plate), and a structural mounting cage to ensure precise alignment and stability.

Regarding the “field of view,” single-vision setups provide a broader theoretical FoV (e.g., $87^\circ \times 58^\circ$ in the RealSense™ D435, shown in Fig. 6-c). However, in dual-vision setups, the beamsplitter’s physical dimensions and the supporting cage partially obstruct the cameras’ FoV, reducing the effective viewing area. For instance, the configuration shown in Fig. 6-c achieves an effective FoV of $57^\circ \times 54.5^\circ$. Another essential factor is “weight”; the static single-vision setup is the lightest, whereas the dynamic single-vision setup adds approximately 30 gr due to the function generator and dynamic polarizer. Thus, single-vision setups are more feasible for minimizing payloads, such as in drones, as dual-vision configurations are heavier. The combined weight of dual-vision setup components typically ranges from 150 to 350 gr, with the plate beamsplitter potentially reducing the overall sensor weight. Finally, considering the noise levels in the processed output, dual-vision setups produce clearer results, isolating only the CSR regions of the

iMarkers. In contrast, the dynamic single-vision setup may introduce additional noise due to motion and illumination fluctuations during “temporal” subtraction. The static single-vision setup retains the highest noise pixels (*i.e.*, pixels that do not contribute to iMarker detection), including the filtered areas with the detected iMarkers.

When choosing among various sensor configurations, a selection parameter is the trade-off between “detection robustness” and “clutter rejection,” as each configuration’s detection pipeline can be tailored to optimize performance for specific application scenarios. Dual-vision setups rely on spatial frame subtraction followed by thresholding, producing cleaner outputs by isolating CSR-coated iMarker regions while effectively suppressing non-marker backgrounds thanks to the differential visibility of CSRs between the two sensor views. However, they are more sensitive to artifacts caused by sensor noise, motion, illumination variations, and frame misalignment. In contrast, single-vision setups may retain more background clutter (noise pixels) alongside detected iMarkers. Accordingly, enhancing robustness and output quality are tackled differently considering the employed sensor variant. While strategies such as adaptive thresholding, active frame registration, and noise modeling can better aid dual-vision setup algorithms, single-vision systems can benefit from lightweight morphological filtering to enhance detection quality without compromising system simplicity.

6.2 Applicability

Considering the unique characteristics of iMarkers, they serve as potential alternatives in scenarios reliant on printed markers. In this regard, the obscure nature of iMarkers makes them appropriate for surroundings with unwanted visual clutter, such as museums, hospitals, offices, *etc.* By safely replacing printed markers, iMarkers can preserve unobtrusiveness and aesthetic integrity while delivering full functionality for robotics and AR systems. It should be noted that various AR applications, particularly those deployable on handheld mobile devices, rely exclusively on RGB cameras and frequently utilize fiducial landmarks to support interactive functionalities like user engagement. This aligns well with the iMarker detection procedure proposed in this paper; specifically the single-vision setup which requires minimal hardware modifications to enable compatibility with standard AR-capable vision sensors.

Additionally, as the iMarker detection pipeline relies on simple computer vision techniques (*e.g.*, thresholding and frame subtraction), it introduces minimal computational overhead and operates efficiently even on a CPU-based system, without requiring hardware acceleration. Thus, the core innovation of the proposed system lies in tightly coupling hardware and software, where the sensor hardware captures frames with filtered views on CSR-coated regions of iMarkers and the software extracts and reveals these regions before passing the result to standard fiducial marker libraries (*e.g.*, ArUco or AprilTag).

Fig. 10 depicts the real-world benchmarking of iMarkers in Visual Simultaneous Localization and Mapping (VSLAM), showcasing the use of a visible-range iMarker to facilitate indoor map reconstruction enriched with semantic information [20]. iMarkers can also be suitable for autonomous robots functioning in retail stores and smart warehousing, where numerous markers are needed to augment objects. Another potential use case includes object grasping in cluttered environments, where iMarkers can supply accurate localization cues to enhance robotic manipulation accuracy. iMarkers can also be strategically employed to seamlessly augment difficult-to-detect objects, like transparent surfaces (*e.g.*, windows and glass block walls), where the transparency poses considerable challenges to computer vision and robot perception systems. Likewise, reflective surfaces, such as mirrors or chrome/metallic objects, often cause distortions or reflections, confusing perception algorithms and negatively impacting object recognition or localization accuracy. In these scenarios, iMarkers can augment such objects by providing reliable information while preserving visual appeal. This allows robots and AR devices to effectively “see” and interact with visually challenging entities, ensuring reliable operation and versatility.

6.3 Limitations and Fabrication Considerations

Given the ongoing nature of this research and the absence of a rapid iMarker fabrication process so far, the experiments remain constrained under varying illumination, weather conditions (for outdoor applications), and environmental factors (*e.g.*, dirt). In terms of environmental robustness, iMarkers are expected to exhibit similar vulnerability to dirt and occlusion as conventional printed markers, since both rely on visual input for marker detection and pose estimation. In other words, the marker recognition pipeline (ArUco in this work) processes either standard RGB frames of normal cameras or the binary outputs of the iMarker detector algorithm, without introducing additional sensitivity. Regarding sunlight and outdoor use, UV-range iMarkers may experience reduced contrast under ambient sunlight, potentially leading to false positives due to uncontrolled UV reflections. Accordingly, the reflectivity of UV-range CSRs needs to be enhanced to ensure that all UV-range iMarkers are reliably detected when illuminated by the light source. Similarly,

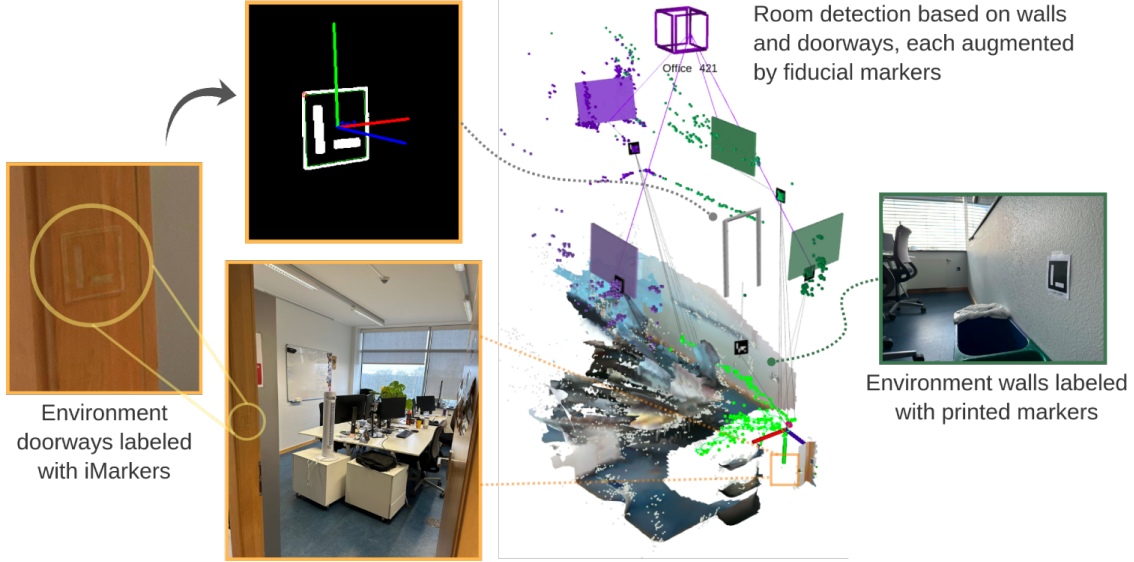


Figure 10: Benchmarking iMarkers for map reconstruction in alliance with printed markers introduced in [20].

IR-range iMarkers could be influenced by environmental IR sources. For these cases in real-world deployments, additional filtering strategies or controlled illumination may be required to ensure reliable iMarker detection.

The scalability of iMarker fabrication for mass deployment is still an active investigation topic. Currently, production involves several manual steps, including microfluidic droplet generation, annealing, polymerization, and sequential washing, which reduce throughput and introduce variability in marker quality. To overcome this, we are developing an integrated, automated production platform that combines all stages into a continuous process with real-time computer monitoring. This system is expected to streamline manufacturing, improve consistency, and enable large-scale high-throughput fabrication suitable for real-world robotics applications.

7 Conclusions

This paper introduced a novel generation of fiducial markers, termed *iMarkers*, designed explicitly for real-world robotics applications. iMarkers are designed to be visually indistinguishable by the human eye, ensuring minimal environmental disruption while remaining fully detectable and recognizable by robots equipped with adequate sensors and adapted detection algorithms. The paper also presents various sensor designs and implemented algorithms for detecting iMarkers placed in the environment and exploiting them for different use cases. Experimental results demonstrate the practicality and potential of these markers as versatile landmarks for data embedding in various real-world scenarios.

Future works include optimizing the iMarker fabrication process to ensure scalable production and enhancing the illumination equipment, sensor designs, and algorithm implementations to guarantee robustness across various scenarios.

Acknowledgments

The authors would like to thank Marco Giberna and Tadej Emersic for their insightful assistance during experiments conducted in this work.

References

[1] M. Kalaitzakis, B. Cain, S. Carroll, A. Ambrosi, C. Whitehead, and N. Vitzilaios, “Fiducial markers for pose estimation: Overview, applications and experimental comparison of the artag, apriltag, aruco and stag markers,”

- [2] G. M. Costa, M. R. Petry, J. G. Martins, and A. P. Moreira, “Assessment of multiple fiducial marker trackers on hololens 2,” *IEEE Access*, 2024.
- [3] N. Ayala, D. Mardanbegi, A. Zafar, E. Niechwiej-Szwedo, S. Cao, S. Kearns, E. Irving, and A. T. Duchowski, “Does fiducial marker visibility impact task performance and information processing in novice and low-time pilots?” *Computers & Graphics*, vol. 119, p. 103889, 2024.
- [4] M. Schwartz, Y. Geng, H. Agha, R. Kizhakidathazhath, D. Liu, G. Lenzini, and J. P. Lagerwall, “Linking physical objects to their digital twins via fiducial markers designed for invisibility to humans,” *Multifunctional Materials*, vol. 4, no. 2, p. 022002, 2021.
- [5] H. Agha, Y. Geng, X. Ma, D. I. Avşar, R. Kizhakidathazhath, Y.-S. Zhang, A. Tourani, H. Bavle, J.-L. Sanchez-Lopez, H. Voos *et al.*, “Unclonable human-invisible machine vision markers leveraging the omnidirectional chiral bragg diffraction of cholesteric spherical reflectors,” *Light: Science & Applications*, vol. 11, no. 1, pp. 1–19, 2022.
- [6] L. Naimark and E. Foxlin, “Circular data matrix fiducial system and robust image processing for a wearable vision-inertial self-tracker,” in *Proceedings. International Symposium on Mixed and Augmented Reality*, 2002, pp. 27–36.
- [7] P. Lightbody, T. Krajník, and M. Hanheide, “A versatile high-performance visual fiducial marker detection system with scalable identity encoding,” in *Proceedings of the Symposium on Applied Computing*, 2017, pp. 276–282.
- [8] F. Bergamasco, A. Albarelli, E. Rodola, and A. Torsello, “Rune-tag: A high accuracy fiducial marker with strong occlusion resilience,” in *2011 IEEE Computer Society Conference on Computer Vision and Pattern Recognition (CVPR’11)*. IEEE, 2011, pp. 113–120.
- [9] H. Kato and M. Billinghurst, “Marker tracking and hmd calibration for a video-based augmented reality conferencing system,” in *Proceedings 2nd IEEE and ACM International Workshop on Augmented Reality (IWAR’99)*. IEEE, 1999, pp. 85–94.
- [10] E. Olson, “Apriltag: A robust and flexible visual fiducial system,” in *2011 IEEE International Conference on Robotics and Automation*. IEEE, 2011, pp. 3400–3407.
- [11] S. Garrido-Jurado, R. Muñoz-Salinas, F. J. Madrid-Cuevas, and M. J. Marín-Jiménez, “Automatic generation and detection of highly reliable fiducial markers under occlusion,” *Pattern Recognition*, vol. 47, no. 6, pp. 2280–2292, 2014.
- [12] R. M. Claro, D. B. Silva, and A. M. Pinto, “Artuga: A novel multimodal fiducial marker for aerial robotics,” *Robotics and Autonomous Systems*, vol. 163, p. 104398, 2023.
- [13] C. Getschmann and F. Echtler, “Seedmarkers: Embeddable markers for physical objects,” in *Proceedings of the Fifteenth International Conference on Tangible, Embedded, and Embodied Interaction*, 2021, pp. 1–11.
- [14] Y. Wang, Y. Ji, D. Liu, Y. Tamura, H. Tsuchiya, A. Yamashita, and H. Asama, “Acmarker: Acoustic camera-based fiducial marker system in underwater environment,” *IEEE Robotics and Automation Letters*, vol. 5, no. 4, pp. 5018–5025, 2020.
- [15] H. Uchiyama and Y. Oyamada, “Transparent random dot markers,” in *2018 24th International Conference on Pattern Recognition (ICPR)*. IEEE, 2018, pp. 254–259.
- [16] M. D. Dogan, A. Taka, M. Lu, Y. Zhu, A. Kumar, A. Gupta, and S. Mueller, “Infraredtags: Embedding invisible ar markers and barcodes using low-cost, infrared-based 3d printing and imaging tools,” in *Proceedings of the 2022 CHI Conference on Human Factors in Computing Systems*, 2022, pp. 1–12.
- [17] M. D. Dogan, R. Garcia-Martin, P. W. Haertel, J. J. O’Keefe, A. Taka, A. Aurora, R. Sanchez-Reillo, and S. Mueller, “Brightmarker: 3d printed fluorescent markers for object tracking,” in *Proceedings of the 36th Annual ACM Symposium on User Interface Software and Technology*, 2023, pp. 1–13.

- [18] D. Li, A. S. Nair, S. K. Nayar, and C. Zheng, “Aircode: Unobtrusive physical tags for digital fabrication,” in *Proceedings of the 30th annual ACM symposium on user interface software and technology*, 2017, pp. 449–460.
- [19] K. D. Willis and A. D. Wilson, “Infrastructs: fabricating information inside physical objects for imaging in the terahertz region,” *ACM Transactions on Graphics (TOG)*, vol. 32, no. 4, pp. 1–10, 2013.
- [20] A. Tourani, H. Bayle, D. I. Avşar, J. L. Sanchez-Lopez, R. Munoz-Salinas, and H. Voos, “Vision-based situational graphs exploiting fiducial markers for the integration of semantic entities,” *Robotics*, vol. 13, no. 7, p. 106, 2024.